



RESEARCH ARTICLE

Generation of 1-MHz, 64-W, 26-fs green pulses via second-harmonic generation of nonlinearly compressed pulses at 1.03 μm

Dongliang Wang^{1,2}, Qi Liu³, Zhongchao Li⁴, Xinyue Yuan^{1,2}, Hongyue Wu^{1,2}, Zixi Liu⁵, Wei Liu^{1,4}, and Guoqing Chang^{1,2,6}

(Received 31 May 2025; revised 11 July 2025; accepted 22 July 2025)

Abstract

High-order harmonic generation (HHG) in noble gases driven by femtosecond lasers is currently a feasible solution to obtain ultrafast pulses in the extreme ultraviolet (EUV) wavelength range. Implementation of high-flux EUV sources requires driving HHG using an ultrafast laser source in the visible wavelength range with MHz repetition rate. In this paper, we employ a multi-pass cell followed by chirped mirrors to compress 1-MHz, 200-W, 300-fs pulses at $1.03~\mu m$ to a duration of 35 fs. The resulting 186-W compressed pulses are focused onto 0.5-mm thick beta barium borate crystal to drive second-harmonic generation and produce positively chirped pulses at 520 nm. These green pulses are de-chirped to 26 fs in duration with an average power of 64 W, which, to the best of our knowledge, represents the highest average power of green pulses with a duration below 100 fs.

Keywords: nonlinear compressor; second-harmonic generation; ultrafast lasers

1. Introduction

Ultrafast extreme ultraviolet (EUV, 10–120 nm) sources with high average power are desired by many scientific applications, such as EUV absorption spectroscopy, EUV-ionization spectroscopy and coherent diffractive imaging of ultrafast magnetization dynamics. For instance, higher EUV power can alleviate space-charge limitations in photoelectron emission spectroscopy at elevated repetition rates^[1], while simultaneously reducing data collection durations and improving signal-to-noise ratios in time-resolved coincidence measurements. High-order harmonic generation (HHG) in noble gases driven by femtosecond lasers is currently a feasible

Correspondence to: W. Liu, School of Science, Sun Yat-sen University, Shenzhen 518107, China. Email: liuwei95@mail.sysu.edu.cn; G. Chang, Beijing National Laboratory for Condensed Matter Physics, Institute of Physics, Chinese Academy of Sciences, Beijing 100190, China. Email: guoqing.chang@iphy.ac.cn

solution to implement ultrafast EUV sources^[2,3]. Since HHG efficiency is highly dependent on the driving laser wavelength known as $\eta \propto \lambda^{-5}$ to $\lambda^{-6[4]}$, using a driving ultrafast laser at a shorter wavelength can significantly improve the HHG yield and produce mW-level EUV pulses^[5–7]. With all other parameters fixed, increasing the driving-laser repetition rate from kHz to MHz can substantially scale up the average power of the resulting EUV source as well.

Ultrafast Ti:sapphire lasers (centered at ~800 nm) are widely employed for driving HHG. However, limited by the lower repetition rate (normally 1–10 kHz), the generated EUV source is below 100 μW per harmonic line [8]. Further power scaling is hindered by the challenges in thermal management of the Ti:sapphire crystal required for increasing the repetition rate. In contrast, ultrafast Yb-doped lasers offer superior thermal dissipation and can operate with average power much higher than what can be achieved by Ti:sapphire lasers, positioning them as a promising

© The Author(s), 2025. Published by Cambridge University Press in association with Chinese Laser Press. This is an Open Access article, distributed under the terms of the Creative Commons Attribution-NonCommercial licence (https://creativecommons.org/licenses/by-nc/4.0), which permits non-commercial re-use, distribution, and reproduction in any medium, provided the original article is properly cited. The written permission of Cambridge University Press must be obtained prior to any commercial use.

¹Beijing National Laboratory for Condensed Matter Physics, Institute of Physics, Chinese Academy of Sciences, Beijing, China

²University of Chinese Academy of Sciences, Beijing, China

³Institute of Advanced Light Source Facilities, Shenzhen, China

⁴School of Science, Sun Yat-sen University, Shenzhen, China

⁵School of Physics, Nankai University, Tianjin, China

⁶Songshan Lake Materials Laboratory, Dongguan, China

D. Wang et al.

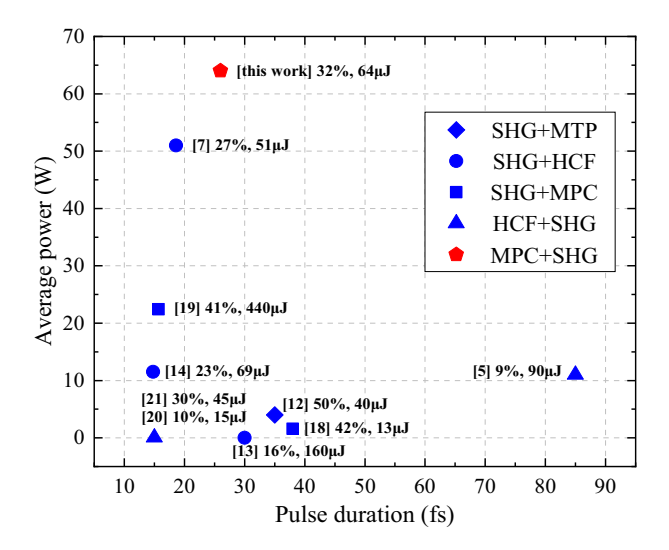


Figure 1. Representative experimental results of the generation of green pulses.

alternative for advancing HHG power^[9]. Notably, Ybdoped rod-type fiber systems currently hold the record for generating more than 10 kW average power in ultrafast laser systems while simultaneously maintaining excellent beam quality^[10]. Ultrafast Yb-doped lasers usually emit pulses at approximately 1.03 µm with a duration longer than 100 fs^[11]. To efficiently driving HHG, conversion of these pulses to a shorter wavelength with a much shorter duration (e.g., <30 fs) is implemented via secondharmonic generation (SHG) in conjunction with pulse postcompression. Figure 1 summarizes the representative results of the current femtosecond sources in the green wavelength range derived from ultrafast Yb-doped lasers. Depending on the sequence of SHG and pulse compression, two main approaches exist to produce energetic femtosecond pulses in the green wavelength range.

(1) Relatively long (>100 fs) green pulses are first generated by SHG and then post-compressed to a much shorter duration. Because the 1.03-µm pulses have a narrow bandwidth (i.e., <10 nm), a thicker SHG crystal can be employed, leading to higher conversion efficiency. The generated SHG pulses have a similar duration to the 1.03-µm pulses. To shorten the pulse duration, the SHG pulses are spectrally broadened in a certain medium - such as multiple thin plates (MTPs), hollow-core fiber (HCF) or a gas-filled multi-pass cell (MPC) - prior to phase compensation by chirped mirrors. The MTP compression features high efficiency while it is only suited for pulse energy below 100 µJ^[12]. Gas-filled HCFs can handle mJ pulse energy despite their relatively low efficiency $(<60\%)^{[7,13,14]}$. For example, Descamps et al.[14] employed HCF for green pulse compression and obtained 15-fs pulses with up to 11.5-W average

power; however, due to the 57% compression efficiency of the HCF, the overall system efficiency was only 23%. Using a similar approach, Klas et al.^[7] employed a Yb-fiber laser with higher average power and achieved 19-fs green pulses at 51 W with a system efficiency of 27%. Further power scaling necessitates active cooling of the fiber and stabilization of the input beam pointing to prevent HCF damage^[15,16]. The MPC has been widely adopted to compress mJ-level pulses at 1.03 µm with average power exceeding 1 kW^[17]. When applied to green pulses, the MPC has a high efficiency (>85%) as well^[18,19]. However, the relatively low damage threshold of optical components in the green wavelength range requires a much larger beam on the MPC cavity mirrors, which increases the overall footprint and complexity of the system. For example, the MPC cavity length when dealing with green pulses of approximately 0.5 mJ energy was close to $2 \, m^{[19]}$.

Before compression, the green pulses directly generated from SHG of 1.03 μm have a typical duration of 200–300 fs. Currently, chirped mirrors with large group-delay dispersion (GDD) (>500 fs²) are absent in the green wavelength range. As a result, more than 15 reflections are usually required to dechirp the spectrally broadened green pulses, which causes power loss and degrades the compression quality.

(2) The 1.03-μm pulses are compressed first to a much shorter duration and followed by SHG to obtain green pulses. The compressed 1.03-μm pulses possess a broader bandwidth, and thus a thinner SHG crystal has to be used in order to convert the full bandwidth. For example, Didenko *et al.*^[20,21] used HCF to spectrally broaden 1.03-μm pulses and potassium dihydrogen phosphate (KDP) crystal for SHG. After de-chirping the green pulses with a prism pair, they obtained 15-fs pulses with up to 45-μJ energy; however, the average power was only 0.45 W. Klas *et al.*^[5] employed beta barium borate (BBO) crystal for SHG and obtained 90-μJ pulses with up to 11-W average power; however, the pulse duration was 85 fs and overall efficiency was only 9%.

In this paper, we employ the MPC to shorten the 1.03-μm pulses delivered by a Yb-fiber laser system, and then use BBO crystal for SHG. Compared with KDP crystal, BBO crystal features thermal robustness, a large nonlinear coefficient and low-pulse temporal walk-off (TW)^[22]. Consequently, our system produces 1-MHz, 64-W, 26-fs pulses centered at 520 nm with a total efficiency of 32%, which, to the best of our knowledge, represents the highest average power of green pulses with a duration below 100 fs.

2. Experimental setup

Figure 2 illustrates our experimental setup. The rod-type Yb-fiber laser system emits 1-MHz, 230-fs pulses centered at 1.03 µm with 200-W average power (corresponding to 200-μJ pulse energy)^[23]. The laser beam is mode matched to the eigenmode of an MPC via three lenses (with focal lengths of 100, -200 and 300 mm) to ensure identical beam properties per pass through the cell. The enclosed Herriottype MPC consists of two identical low-dispersion mirrors (0.3 m in radius of curvature and 50.8 mm in diameter) separated by 0.586 m. The calculated Gaussian eigenmode has a 1/e² diameter of 0.24 mm at the focal plane and 1.6 mm on the mirrors. The MPC is filled with 3-bar (1 bar = 0.1 MPa) krypton gas and the pulse spectrum is significantly broadened after 23 focal passes. Matching the collimated beam to the linear eigenmode of the MPC and re-collimating the beam after passing through the cell is realized by one plano-convex lens (focal length of 800 mm). After the MPC, the spectrally broadened pulses with 186-W average power are de-chirped by four chirped mirrors, which provide a total GDD of -3500 fs². The de-chirped pulses are reduced to 2.5 mm in beam diameter by a combination of the L5 lens (150-mm focal length) and the L6 lens (-75-mm focal length).

Efficient generation of green pulses via SHG from 1.03-μm femtosecond pulses at 186 W needs the careful selection of proper nonlinear crystal. In the small-signal model without considering depletion of the fundamental wave, SHG efficiency can be estimated as

$$\eta = \frac{8\pi^2 d_{\text{eff}}^2 L^2 I_{\omega}}{\varepsilon_0 c^3 n_{\omega}^2 n_{2\omega} \lambda_{\omega}^2} \cdot \text{sinc}^2 \left(\frac{\Delta k L}{2}\right),$$

where η is the SHG efficiency, $d_{\rm eff}$ is the effective nonlinear coefficient, L is the crystal thickness, I_{ω} is the intensity

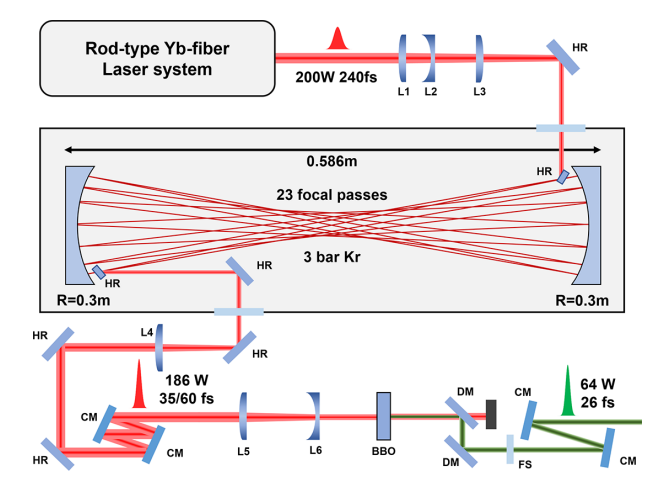


Figure 2. Schematic of the experimental setup. L, lens; HR, high-reflection mirror; CM, chirped mirror; BBO, nonlinear crystal (beta barium borate); DM, dichroic mirror; FS, fused silica.

Table 1. Comparison of SHG performance among typical nonlinear crystals^a.

		$d_{ m eff}$	PB	TW	TT	FOM
Crystal	PT	(pm/V)	$(GHz{\cdot}cm)$	(fs/mm)	$(K \cdot cm)$	$(10^{18} \text{ pm}^3/\text{V}^2)$
BBO	oo→e	2.01	527	93	37.7	3.44
LBO	$oo \rightarrow e$	0.83	971	53	7.02	2.06
BIBO	$ee \rightarrow o$	3.40	260	193	2.68	1.77
KDP	$oo{\to}e$	0.27	37,677	1.3	11.2	3.31
KTP	$eo{\rightarrow}e$	2.80	110/384	458/134	40.7	2.50
CLBO	$oo{\to}e$	0.39	1090	47	53.6	0.78
CBO	$ee{\to}o$	1.01	634	80	109.6	1.54

^aPT, phase-matching type; $d_{\rm eff}$, effective nonlinear coefficient; PB, phase-matching bandwidth; TW, temporal walk-off; TT, temperature tolerance; FOM = $\frac{8\pi^2 d_{\rm eff}^2 L^2}{n_{\omega}^2 n_{2\omega}} \cdot {\rm sinc}^2 \left(\frac{\Delta k L}{2}\right)$. (PB and temperatures are ranges over which $L\Delta k$ varies from $-\pi$ to π . This is 13% greater than the full width at half maximum for sinc² (ΔkL/2) function that describes SHG efficiency. $\lambda_{\omega}=1030$ nm, $\lambda_{2\omega}=515$ nm, T=300 K.)

at fundamental frequency, $\Delta k = 2k_{\omega} - k_{2\omega}$ is the phase mismatch at central frequencies, n_{ω} and $n_{2\omega}$ are the refractive indices of the corresponding frequencies and λ_{ω} is the fundamental wavelength. To quantify the dependence of SHG efficiency on the nonlinear crystal, a figure of merit (FOM) can be defined as

$$\text{FOM} = \frac{8\pi^2 d_{\text{eff}}^2 L^2}{n_{\omega}^2 n_{2\omega}} \cdot \text{sinc}^2 \left(\frac{\Delta kL}{2}\right).$$

Table 1 presents a comparison of optical properties of seven crystals commonly used for SHG. For frequency doubling of high-power broadband (>40 nm) femtosecond pulses at 1.03 μ m, the crystal thickness is usually less than 1 mm to provide enough phase-matching bandwidth (PB). In this scenario, spatial walk-off between the input pulses and the SHG pulses is minimal and thus not included in the table. Columns 3–6 list the effective nonlinear coefficient ($d_{\rm eff}$), PB, TW and temperature tolerance (TT). TT is defined as the ratio between the temperature change and the wave-vector mismatch, which quantifies the variation of phase mismatch due to temperature rise in the crystal. A crystal with larger TT is beneficial when applied to SHG of femtosecond pulses with high average power (i.e., >100 W).

An ideal SHG crystal should simultaneously exhibit low TW, large $d_{\rm eff}$, broad PB and large TT. To have a fair comparison, we calculate the FOM of the listed crystals for frequency doubling of 30-fs pulses centered at 1.03 μ m (the spectral bandwidth is about 14,200 GHz). Here, L is estimated as PB/14,200. We assume that Δk is caused by a temperature rise of 30 K, that is, $\Delta k = 30/\text{TT}$. The last column in Table 1 shows the calculated FOM for each crystal. BBO crystal exhibits the largest FOM; together with a high damage threshold, BBO crystal is good choice for frequency doubling high-power femtosecond pulses with a broad bandwidth. KDP has a comparable FOM to BBO;

D. Wang et al.

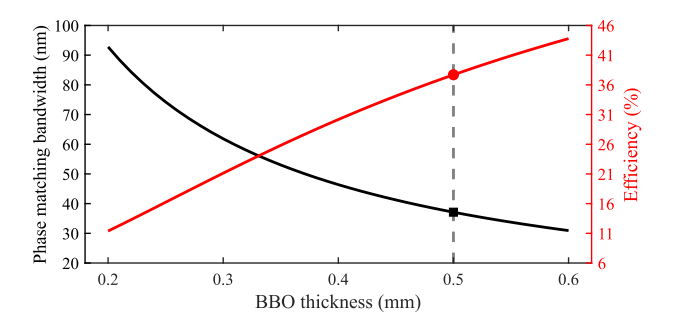


Figure 3. Phase-matching bandwidth (black) and SHG efficiency (red) versus BBO thickness. Gray dotted line marks the phase-matching bandwidth and SHG efficiency of 0.5-mm thick BBO.

however, KDP crystal features a damage threshold two orders of magnitude lower compared with BBO crystal^[24]. The SHG average power obtained based on KDP crystals is usually less than 1 W.

We calculate the conversion efficiency at various crystal thicknesses by numerically solving the coupled-wave equations for frequency doubling 1.03-μm, 30-fs pulses with 185-μJ pulse energy and 3-mm beam diameter in BBO crystal. The red curve in Figure 3 shows the conversion efficiency as a function of BBO thickness, and the black curve shows the corresponding PB. As expected, increasing the crystal thickness improves the SHG efficiency accompanied by a reduced PB. A 0.5-mm thick BBO crystal (indicated by the gray dashed line) appears to be an optimal choice because it provides enough PB (36 nm) to support green pulses with less than 30 fs duration; meanwhile, it corresponds to a high conversion efficiency of 37%. Guided by the above analysis, we experimentally choose a 0.5-mm-thick BBO crystal to

perform SHG followed by completely separating the SHG pulses from the input 1.03-µm pulses using dichroic mirrors.

3. Results and discussion

As the pulse propagates inside the MPC, the accumulated nonlinear phase – which is proportional to the pulse energy and the nonlinear coefficient (or gas pressure) – results in a broadened optical spectrum that in turn determines the transform-limited (TL) pulse duration^[25]. Figure 4(a) plots the broadened spectra at the MPC output measured at 100 μ J with the Kr pressure increased from 1.5 to 4.5 bar (with intervals of 0.5 bar). As Figure 4(b) shows, the corresponding TL pulse duration calculated from the measured spectra drops from 130 to 53 fs. In another experiment, we fix the Kr pressure at 3 bar and measure the broadened spectra with the pulse energy increased from 50 to 200 μ J (Figure 4(c)); the corresponding TL pulse duration decreases from 126 to 31 fs (Figure 4(d)).

The peak power on the concave mirror of the MPC is up to 200 GW/cm², well below the damage threshold. Figure 5(a) shows MPC output power and efficiency versus input power. At the highest input power of 200 W, the MPC output power is 186 W. The efficiency of the MPC is more than 90% at all powers. Due to a long optical path of 18.5 m, the optical beam at the MPC output exhibits noticeable pointing fluctuation. To meet the requirement for driving HHG, we add a pointing stabilization device, which consists of two actuators and two four-quadrant-diode detectors. The pointing results are shown in Figures 5(b) and 5(c). The measurement uses a 200-mm lens to focus the spot, and charge-coupled device (CCD) camera samples at 5 Hz for

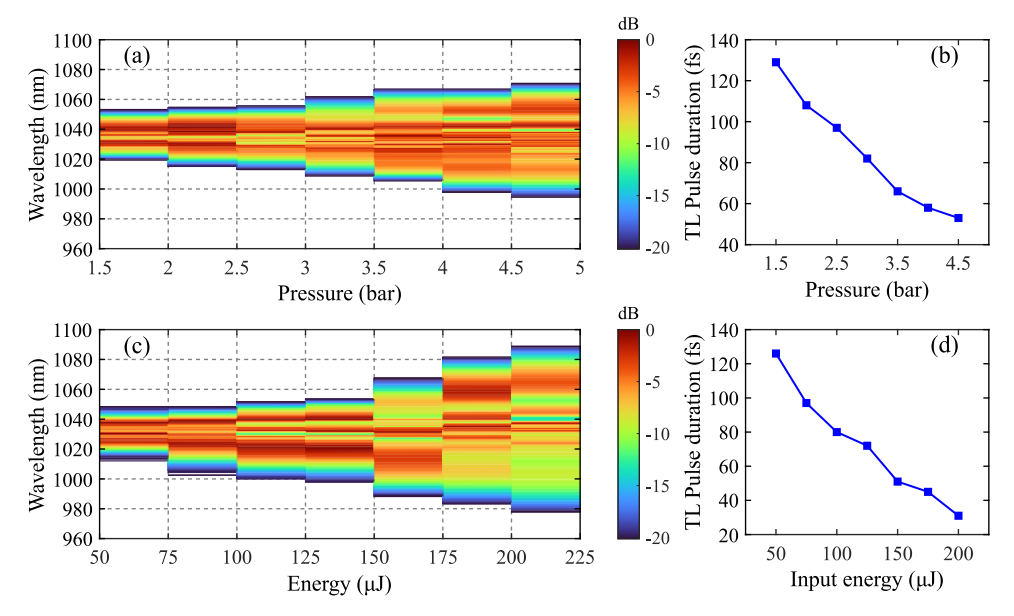


Figure 4. Broadened spectra and TL pulse duration at different pressures and input energies. Broadened spectra (a) and TL pulse duration (b) at 1.5–4.5 bar Kr pressure at 100 μ J input energy. Broadened spectra (c) and TL pulse duration (d) at 50–200 μ J input energy at 3 bar pressure.

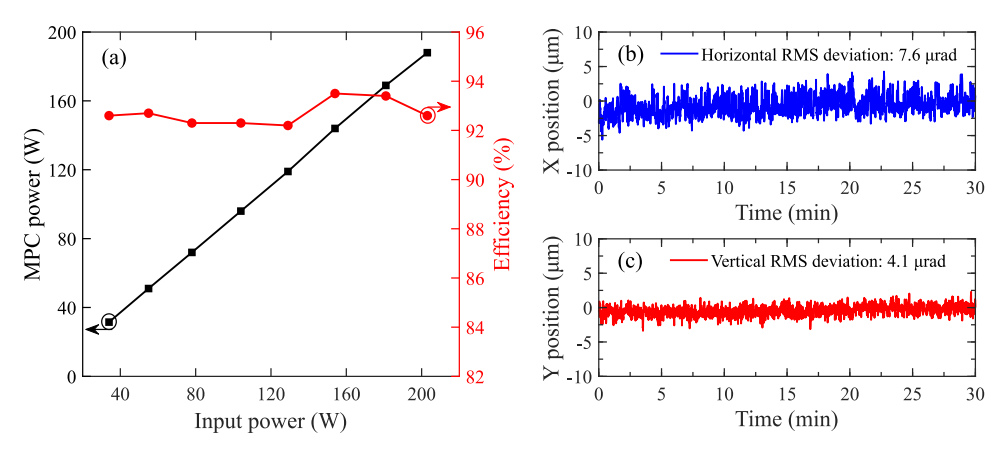


Figure 5. (a) MPC output power and efficiency versus input power. Horizontal (b) and vertical (c) beam angular pointing stability.

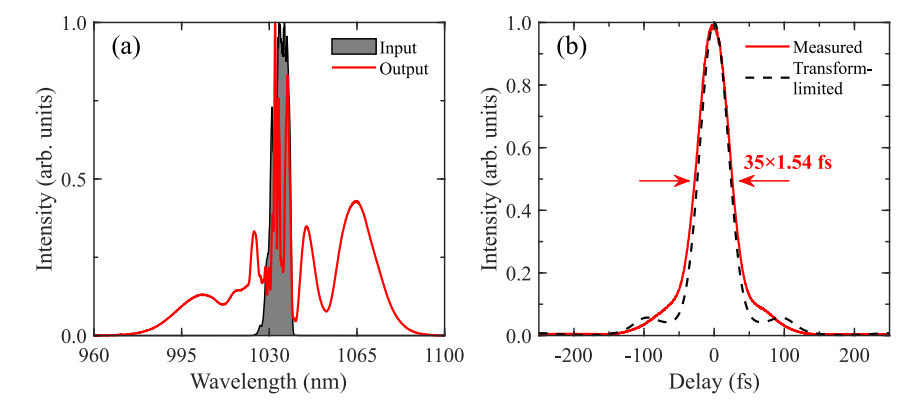


Figure 6. (a) Input (gray shading) and output (red) spectra of the MPC. (b) Measured autocorrelation trace (red) and calculated autocorrelation trace of the TL pulse (black dashed).

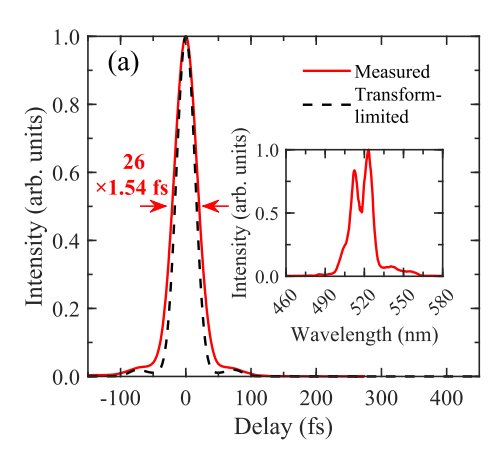
30 min. The root mean square (RMS) values of the focal spot shift over 30 min are 1.5 and $0.8~\mu m$. Horizontal and vertical RMS deviations are 7.6 and 4.1 $\mu rad,$ which represents about a 2.6 times reduction compared with the case without pointing stabilization.

The red curve in Figure 6(a) shows the MPC output spectrum at 200-W input power with the Kr pressure set at 3 bar (Yokogawa, AQ6370D, resolution 0.2 nm). The input spectrum with a spectral width of 8.1 nm (gray shading area in Figure 6(a)) is significantly broadened spanning 980–1080 nm. The spectrally broadened pulses are then dechirped by chirped mirrors that provide –3500 fs² GDD. The red curve in Figure 6(b) plots the measured autocorrelation trace of the de-chirped pulse with an estimated duration of 35 fs. Also plotted in the same figure is the calculated autocorrelation trace of the corresponding TL pulses (black dashed curve) with a duration of 31 fs, and the de-chirped pulses are close to being TL.

A 0.5-mm-thick BBO crystal cut for type-I phase matching (phase-matching angle at 23.4°) is used to convert the 186-W compressed pulses to the green spectral range via SHG. The TW between the 1.03- μm pulse and the SHG pulse in the BBO crystal is 93 fs/mm, which reduces the conversion efficiency and narrows the SHG spectrum. This adverse

effect can be mitigated by slightly pre-chirping the input 1.03-µm pulse. In our experiments, we intentionally add approximately 400 fs² GDD to the 1.03-um compressed pulse (i.e., the measured pulse in Figure 6(b)) in order to stretch it to a duration of about 60 fs. For type-I SHG at 1030 nm in a 0.5-mm BBO crystal, the walk-off angle of 57 mrad yields a spatial displacement of approximately 0.03 mm between the fundamental and SHG beams. Such a displacement is negligible relative to the fundamental beam diameter of 2.5 mm, which has little impact on the conversion efficiency. In this scenario, the resulting SHG pulses have 66-W average power (corresponding to 36% conversion efficiency) with a duration of 78 fs; the inset of Figure 7(a) shows the SHG spectrum with a spectral width of 18 nm (Avantes, AvaSpec-3648, resolution 0.33 nm). The SHG pulses are compressed by two chirped mirrors designed to provide -100-fs² GDD per reflection over the spectral range from 490 to 540 nm. The compressed pulse duration drops from 78 to 60 fs (32 fs) corresponding to the compensated GDD at -200 fs^2 (-400 fs^2). To achieve the shortest pulse duration, we place a 2-mm-thick fused-silica plate before the chirped mirrors for finely tuning GDD compensation. With a total GDD of -540 fs², the SHG pulses are compressed down to 26 fs (red curve in Figure 7(a)). The black dashed

6 D. Wang et al.



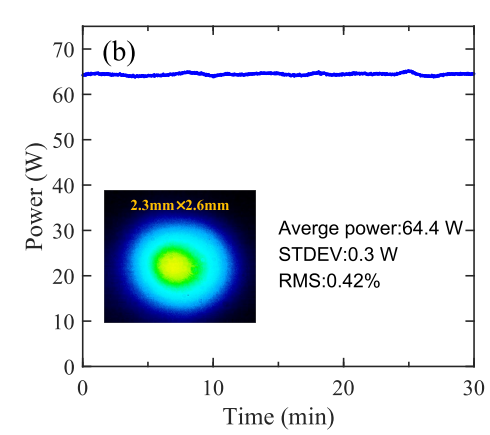


Figure 7. (a) Measured autocorrelation trace (red) and calculated autocorrelation trace of the TL pulse (black dashed). Inset: SHG spectrum. (b) Average power stability of the compressed SH pulses. Inset: SHG beam profile.

curve in the same figure is the calculated autocorrelation trace of the corresponding TL pulses. The TL pulses have a duration of 24 fs, and the de-chirped pulses are close to being TL. We measure the average power stability of 64-W compressed pulses over 30 min, and the RMS of the average power is below 0.42% (Figure 7(b)). The inset of Figure 7(b) shows a Gaussian-like spatial profile, indicating an excellent beam quality. The reduction in beam ellipticity (compared to the spot of the front-end laser) is attributed to a minor mode mismatch within the MPC under high-power conditions.

4. Conclusion

We implement a powerful ultrafast HHG driving source at the green wavelength, which is based on a Yb-fiber laser system that emits 1-MHz, 200-W, 230-fs pulses centered at 1.03 μ m. These pulses are shortened by an MPC compressor and then frequency doubled in a BBO crystal. Centered in the green wavelength range, the generated SHG pulses are 26 fs in duration with 64-W average power (corresponding to 64- μ J pulse energy). Ongoing work is to employ this green source to drive HHG to produce EUV pulses with mW average power.

In recent years, the rapid development of high-power Yb-fiber laser systems $^{[26]}$ and high-power MPC compression technology has made it possible to obtain 1004-W, 31-fs pulses at 1.03 $\mu m^{[17]}$. Frequency doubling at the kW power level in BBO causes a thermal gradient that in turn degrades the beam quality $^{[27,28]}$. Bonding sapphire with large thermal conductivity can effectively mitigate the thermal effect of the crystal without compromising the SHG efficiency. As a result, it is feasible to produce green pulses with less than 30-fs duration and hundreds of watts average power, which constitutes an enabling HHG driving source to achieve high-flux EUV pulses.

Acknowledgement

This work is supported by the Key Deployment Special Research Project of the Chinese Academy of Sciences (Grant No. PTYQ2022YZ0001) and the National Natural Science Foundation of China (Grant Nos. 62175255 and 62227822).

References

- M. Keunecke, C. Moller, D. Schmitt, H. Nolte, G. S. M. Jansen, M. Reutzel, M. Gutberlet, G. Halasi, D. Steil, S. Steil, and S. Mathias, Rev. Sci. Instrum. 91, 063905 (2020).
- A. Mcpherson, G. Gibson, H. Jara, U. Johann, T. S. Luk, I. A. Mcintyre, K. Boyer, and C. K. Rhodes, J. Opt. Soc. Am. B 4, 595 (1987).
- 3. M. Ferray, A. Lhuillier, X. F. Li, L. A. Lompre, G. Mainfray, and C. Manus, J. Phys. B 21, L31 (1988).
- A. D. Shiner, C. Trallero-Herrero, N. Kajumba, H. C. Bandulet, D. Comtois, F. Legare, M. Giguere, J. C. Kieffer, P. B. Corkum, and D. M. Villeneuve, Phys. Rev. Lett. 103, 073902 (2009)
- R. Klas, S. Demmler, M. Tschernajew, S. Hädrich, Y. Shamir, A. Tünnermann, J. Rothhardt, and J. Limpert, Optica 3, 1167 (2016).
- A. Comby, D. Descamps, S. Beauvarlet, A. Gonzalez, F. Guichard, S. Petit, Y. Zaouter, and Y. Mairesse, Opt. Express 27, 20383 (2019).
- R. Klas, A. Kirsche, M. Gebhardt, J. Buldt, H. Stark, S. Hädrich, J. Rothhardt, and J. Limpert, PhotoniX 2, 4 (2021).
- J. Lee, D. R. Carlson, and R. J. Jones, Opt. Express 19, 23315 (2011).
- 9. G. Chang and Z. Wei, iScience 23, 101101 (2020).
- M. Muller, C. Aleshire, A. Klenke, E. Haddad, F. Legare, A. Tunnermann, and J. Limpert, Opt. Lett. 45, 3083 (2020).
- V. Hilbert, M. Tschernajew, R. Klas, J. Limpert, and J. Rothhardt, AIP Adv. 10, 045227 (2020).
- S. Wang, J. Yan, S. Song, A. Atanassov, Z. Wu, W. Brunner, D. Popmintchev, and T. Popmintchev, arXiv:2307.01164 (2023).
- 13. J. Xia, C. Altucci, S. Amoruso, R. Bruzzese, R. Velotta, and X. Wang, Opt. Express 16, 3527 (2008).

- D. Descamps, F. Guichard, S. Petit, S. Beauvarlet, A. Comby, L. Lavenu, and Y. Zaouter, Opt. Lett. 46, 1804 (2021).
- S. Hädrich, A. Klenke, A. Hoffmann, T. Eidam, T. Gottschall, J. Rothhardt, J. Limpert, and A. Tünnermann, Opt. Lett. 38, 3866 (2013).
- T. Nagy, S. Hädrich, P. Simon, A. Blumenstein, N. Walther, R. Klas, J. Buldt, H. Stark, S. Breitkopf, P. Jójárt, I. Seres, Z. Várallyay, T. Eidam, and J. Limpert, Optica 6, 1423 (2019).
- C. Grebing, M. Müller, J. Buldt, H. Stark, and J. Limpert, Opt. Lett. 45, 6250 (2020).
- V. Hariton, A. Bin Wahid, G. Figueira, K. Fritsch, and O. Pronin, Opt. Lett. 47, 1246 (2022).
- 19. M. Karst, P. Pfaller, R. Klas, Z. Wang, P. Gierschke, J. Rothhardt, and J. Limpert, Opt. Lett. 48, 1300 (2023).
- N. V. Didenko, A. V. Konyashchenko, L. L. Losev, V. S. Pazyuk, and S. Y. Tenyakov, Opt. Commun. 282, 997 (2009).
- N. V. Didenko, A. V. Konyashchenko, P. V. Kostryukov, L. L. Losev, and S. Y. Tenyakov, Quantum Electron. 41, 804 (2011).

- R. Riedel, J. Rothhardt, K. Beil, B. Gronloh, A. Klenke, H. Hoppner, M. Schulz, U. Teubner, C. Krankel, J. Limpert, A. Tunnermann, M. J. Prandolini, and F. Tavella, Opt. Express 22, 17607 (2014).
- 23. D.-L. Wang, Z. Shi, J.-S. Wang, H.-Y. Wu, X.-H. Zhang, and G.-Q. Chang, Acta Phys. Sin. **73**, 134204 (2024).
- H. Yoshida, H. Fujita, M. Nakatsuka, M. Yoshimura, T. Sasaki, T. Kamimura, and K. Yoshida, Jpn. J. Appl. Phys. 45, 766 (2006).
- 25. A. L. Viotti, M. Seidel, E. Escoto, S. Rajhans, W. P. Leemans, I. Hartl, and C. M. Heyl, Optica 9, 197 (2022).
- H. Fathi, M. Naerhi, and R. Gumenyuk, Photonics 8, 566 (2021).
- C. Rothhardt, J. Rothhardt, A. Klenke, T. Peschel, R. Eberhardt, J. Limpert, and A. Tünnermann, Opt. Mater. Express 4, 1092 (2014).
- J. Rothhardt, C. Rothhardt, M. Muller, A. Klenke, M. Kienel,
 S. Demmler, T. Elsmann, M. Rothhardt, J. Limpert, and A. Tunnermann, Opt. Lett. 41, 1885 (2016).